

## Enhancement of automatic classification of arcus senilis-nonarcus senilis using convolutional neural network

Nur Farahin Bt Abdul Halim<sup>1</sup>, Ridza Azri Bin Ramlee<sup>1,3</sup>, Mohd Zaki Bin Mas'ud<sup>2</sup>, Amirul Jamaludin<sup>1</sup>

<sup>1</sup>Faculty of Electronics and Computer Engineering, Universiti Teknikal Malaysia Melaka (UTeM), Durian Tunggal, Melaka, Malaysia

<sup>2</sup>Faculty of Information and Communication Technology, UTeM, Durian Tunggal, Melaka, Malaysia

<sup>3</sup>Advanced Sensors Embedded Control System Research Group (ASECs), UTeM, Durian Tunggal, Melaka, Malaysia

### Article Info

#### Article history:

Received Nov 29, 2021

Revised Jul 2, 2022

Accepted Jul 28, 2022

#### Keywords:

Cholesterol

Corneal arcus

Convolutional neural network

Deep learning

Non-invasive

### ABSTRACT

Cholesterol is a type of lipid found in the human body and is susceptible to abnormalities. It can be detected via lipid profiling through blood sampling. In addition, cholesterol can be detected through the presence of a "sodium ring" in the eye iris called the corneal arcus (CA), presenting a new preliminary detection method that is less invasive. Therefore, this paper proposed a non-invasive method in detecting cholesterol based on convolutional neural network (CNN) model representation using 300 normal and 300 abnormal iris images from UBIRIS and medical web images. In this work, contrast-limited adaptive histogram (CLAHE) and unsharp masking process was applied first on CA images to enhance the quality of CA images. To detect the CA images, the dataset was trained and tested using three pre-trained CNN architectures; one is created from scratch, another are Resnet-50 and VGG-19 architectures that were fine-tuned to the CA images. The best result was exhibited by proposed pre-trained CNN model created from scratch with 10-fold cross-validation that produced high average detection accuracy at 98.81%. Thus, deeper network implementation is recommended in the future to further improve CA localization for optometrists used in their daily clinical tasks in detecting cholesterol.

*This is an open access article under the [CC BY-SA](#) license.*



### Corresponding Author:

Ridza Azri Bin Ramlee

Faculty of Electronics and Computer Engineering, Universiti Teknikal Malaysia Melaka

76100 Durian Tunggal, Malaysia

Email: ridza@utem.edu.my

## 1. INTRODUCTION

A balanced lifestyle reflects an individual's physical and emotional well-being, which are inextricably linked in many cases. One of the most common physical health problems is high and low cholesterol in the blood vessels. Excessive cholesterol levels can lead to cardiovascular diseases such as stroke, high blood pressure, and myocardial infarction, hence the need to maintain a healthy blood cholesterol level. An individual's cholesterol level is determined using a lipid panel or a lipid profile via a blood test performed after fasting for nine to 12 hours. However, it is considered an invasive method since its sole purpose, in this case, is to obtain a lipid profile. There are many examples of non-invasive techniques in disease diagnosis. For instance, the x-ray is used to view the images of bones and other structures in the body, while magnetic resonance imaging (MRI) creates accurate images of the body's organs and tissues, and computerised tomography (CT) scan detects abnormalities in the body. Thus, it is highly possible to develop an alternative, non-invasive method for detecting cholesterol for preliminary diagnosis rather than using the lipid profile, even though it does not indicate the level of high-density lipoprotein (HDL) or low-density lipoprotein (LDL) at this stage. With this invention, monitoring cholesterol levels would become more

convenient and a step towards living a healthier lifestyle. Therefore, there is a need for a less invasive cholesterol test like iridology technique that can help doctors identify patients with high cholesterol without taking a single drop of blood.

Iridology is a technique that was discovered more than a century ago to discover information about a person's health by evaluating iris features such as color or pattern [1], [2]. The high level of cholesterol in the human body is one of the disorders that are identifiable using the iridology approach [3]. High level of cholesterol or lipid can change the iris pattern, a disorder referred to CA. Cholesterol deposition in the peripheral cornea occurs as a grey-white or yellowish opacity near the cornea's periphery, separated from the limbic margin by a clear corneal region known as the lucid interval [4]. CA is mostly reported in senior citizens, especially those aged 50 and up [5], and its incidence is rare in those under the age of 40 [6]. Urbano [5], lipid thickness usually ranges from 0.3 to 1 mm in width. A study by Meyer *et al.* [7] stated that the corneal lesions found in CA strongly resemble the vessel wall changes found in atherosclerotic lesions, suggesting its correlation with dyslipidemia patients. Figure 1 and 2 shows the differences between normal and abnormal eye.



Figure 1. The normal eye

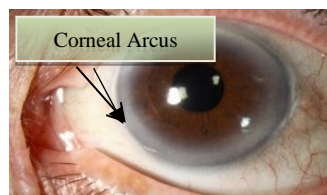


Figure 2. CA infected eye image [8]

The rapid advancement of machine learning (ML) and image oriented deep learning (DL) is enabling for the development of solutions for increasingly complicated challenges. Artificial intelligence (AI) is becoming more appealing for medical applications, enabling for the exploration of new areas where computer algorithms might improve medical operations [9]-[12], also recent world-wide disease namely COVID-19 that has been declared as a pandemic by the World Health Organization on 11<sup>th</sup> March 2020 [13]-[16]. Recent studies have demonstrated the potential of various non-invasive techniques in detecting cholesterol from the images of iris [1], [17]-[21], skin [22], [23], MRI [24], and hand pattern [25]. Most of these methods are based on ML algorithms that extract all the image features before training the dataset. Currently, there are a few computer-assisted cholesterol detection technologies based on the DL technique. Banowati *et al.* developed an application that can detect CA by using android smartphone camera. They applied pre-trained Inception-v3 architectures with 10-fold cross validation in classifying normal eye and CA images [21]. Putri and Saputro [20] proposed a CNN model consists of 20 hidden layers with four convolution layers to classify LDL level status into two classes (High LDL and Normal LDL). The authors also tested the dataset on autoencoder CNN then compared with the proposed CNN to analyse training and testing the complexity and the performance of the model in terms of accuracy. The proposed CNN model has yielded 97.14% classification accuracy [20]. Amini & Ameri applied AlexNet and VGG-16 pre-trained CNN architectures with 4-fold cross-validation into normal and CA images using transfer learning approach [1]. Kocejko *et al.* [9] used CNN automatic identification of the CA presence. On top of that, the author also used neural network models based on the VGG16, ResNet and Inception architectures. The performance of the models was evaluated on a set of images acquired from volunteers with a custom mobile application. They achieved accuracy of 88% for CA detection in a real-life scenario and F1 score of 86% [9].

In this study, we have proposed deep CNN model created from scratch aimed to classify normal and CA images. In comparison to the proposed method, two well-known pre-trained CNN models, ResNet-50 and VGG-19 were fine-tuned based on the dataset and used as deep models. The approach proposed in this study does not require any preprocessing or manual feature extraction techniques. Using normal and CA raw images as input, the classification and feature extraction processes were completed automatically in an end-to-end framework. The main contributions of this study can be summarized as:

- The fine-tuned CNN (proposed method), Resnet-50 and VGG-19 pre-trained models are proposed to classify normal and CA images automatically.
- The CNN (proposed method) pre-trained models demonstrated a better classification accuracy then the well-known pre-trained CNN model namely Resnet-50 and VGG-19.
- The suggested method is a strong and state-of-the-art method in classifying normal and CA images in the medical field.

The rest of the paper is organized as follows: the methodology is presented in section 2. Section 3 discusses the obtained results are presented in section 2 and the whole paper is concluded in section 4.

**2. PROPOSED MATERIALS AND METHOD CORNEAL ARCUS CLASSIFICATION**

**2.1. Data collection and preparation**

Image acquisition is the action of retrieving an image from a source in image processing and machine vision, which is typically hardware systems such as cameras, sensors, and so on. Proença *et al.* [26] stated that the normal eye dataset can be obtain from seven free accessible iris picture databases that can be utilised for biometric purposes. In this study, a dataset of 150 eye images was used in this study: 75 images each for normal and abnormal eyes referred to as CA images. Moreover, the normal eye images were obtained from UBIRIS [26], which is a public database of eye images, while the abnormal eye images were obtained from different public medical sites.

**2.2. Image pre-processing**

**2.2.1. Image augmentation**

Data augmentation was used in this study to improve classification system and prevent the overfitting while training the network. In this study, the 150 original images of CA were rotated at 180° and all images were resized to 224x224 pixels to standardise the image sizes while keeping the aspect ratio of the original image. Figures 3 and 4 shows the sample abnormal image before and after 180° rotation of an eye image. In total, a dataset of 300 images were formed and ready to train using the proposed network. Besides, this study also experimenting grey scale representation of the 300 eye images for both normal and abnormal eye dataset. Figure 5 and 6 illustrate a sample of proposed dataset normal and abnormal eye.



Figure 3. The original CA infected eye image [8]      Figure 4. A sample of horizontal rotation

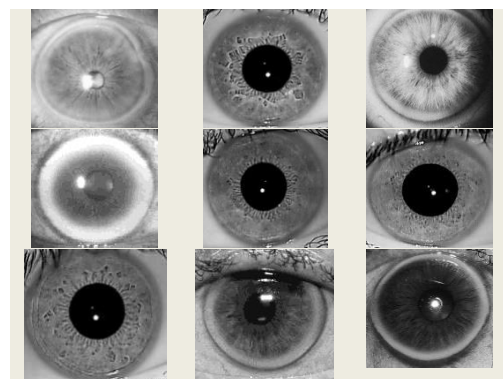


Figure 5. RGB Normal and CA eye images with 224x224 pixels

Figure 6. Gray scale normal and CA eye images with 224x224 pixels

**2.2.2. Image quality enhancement**

In this work, CLAHE and unsharp masking process was applied on CA images to enhance the quality of CA images. CLAHE was mainly applied for the improvement of low-contrast medical images [28], [29]. The CLAHE introduced clipping limit to address the issue of the noise amplification problem [30]. The CLAHE method uses the histogram equalization to each contextual region. The original histogram is clipped, and redistributed to each grey level. The sharpening process works by using the slightly blurred version of the original image. Then, the unsharp mask is then created by subtracting this from the original to identify the

presence of edges, creating the unsharp mask (effectively a high pass filter). The CLAHE and unsharp masking method to enhance the original image are as in (1)-(9):

Step 1: Calculating the average number of pixels per region.

$$N_A = \frac{(N_X \times N_Y)}{N_G} \quad (1)$$

$N_A$  is the average number of pixels,  $N_X$  and  $N_Y$  is the number of pixels in the X and Y dimension,  $N_G$  is the number of gray levels.

Step 2: The actual clip limit can be expressed.

$$N_A = N_X \times N_{NCL} \quad (2)$$

$N_{NCL}$  is the clip limit that normalized clip limit in the range of 0 until 1.

Step 3: The clip limit is used for the height of histogram.

$$H_i = \begin{cases} N_{NCL} & \text{if } N_i \geq N_{NCL} \\ N_i & \text{else} \end{cases} \quad i = 1, 2, \dots, l - 1 \quad (3)$$

$H_i$ ,  $N_i$ ,  $l$  is the height of the histogram of iteration per tile, the histogram of iteration tile and the number of gray levels respectively.

Step 4: The average of the remain pixels to distribute to each gray level.

$$N_C = (N_X \times N_Y) \sum_{i=0}^{l-1} H_i \quad (4)$$

The number of clipped pixels is denoted as  $N_C$ .

Step 5: The number of pixels to be redistributed.

$$N_R = \frac{N_C}{L} \quad (5)$$

The pixels can be redistributed either in a uniformly or non-uniformly. The number of pixels to be redistributed as  $N_R$ . The number of undistributed pixels is computed as in (4) and (5) until all pixels are redistributed as in (6) is repeatedly.

$$H_i = \begin{cases} N_{NCL} & \text{if } N_i + N_R \geq N_{NCL} \\ N_i + N_R & \text{else} \end{cases} \quad i = 1, 2, \dots, l - 1 \quad (6)$$

Step 6: Cumulative histogram of the contextual region.

$$C_i = \left( \frac{1}{(N_X \times N_Y)} \right) \sum_{j=0}^i H_j \quad (7)$$

The histogram of the contextual region is matched with uniform, Rayleigh, or exponential probability distributions once all computations are completed, resulting in a defined brightness and visual quality. Assuming we have a pixel P (x, y) with a value of s and four center points R 1, R 2, R 3 and R 4 that correspond to the neighbor tiles. Over these four contextual areas, a weighted total is computed. The tiles are blended for the output image, and bilinear interpolation is used to remove blemishes between the independent tiles. The new value of s, represented as s', is derived from (8).

$$S' = (1 - y)((1 - x) \times R_1(s) + x \times R_2(s)) + y((1 - x) \times R_3(s) + x \times R_4(s)) \quad (8)$$

Step 7: The traditional unsharp masking

$$y(m, n) = x(m, n) + \lambda(m, n) \times z(m, n) \quad (9)$$

In the formula (9),  $x(m, n)$  is the original image signal,  $y(m, n)$  is the enhanced image signal,  $z(m, n)$  is the enhancement operator,  $\lambda(m, n)$  is the enhancement coefficient and is used to control the degree of enhancement, denote  $\lambda(m, n) > 0$ .  $z(m, n)$  often has the rotational invariance.

After these steps, the enhanced image can be obtained. Figure 7 and 8 shows a result of image quality enhancement using CLAHE and unsharp masking process.



Figure 7. The original abnormal image



Figure 8. The abnormal image after using proposed method of image enhancement

### 2.3. Model architecture and feature extraction

In this analytical study, the MATLAB R2020b programmed was used in developing the proposed method. The training data is further divided into two parts: Training and validation data with a ratio of 70% and 30%, respectively, to determine if the model exhibits overfitting. This study utilized a pre-trained CNN (proposed method), ResNet-50 and VGG-19 models trained with 10-fold cross validation on normal and CA dataset and fine-tuned based on the training images. Initially, different CNN architectures are employed for feature extraction, which are combined into three fully connected layers for classification tasks. The combined features contain multiple features extracted from a single descriptor. These features may represent to express shape descriptors like circularity, roundness, and compactness [31]. In the proposed framework, two well-known pre-trained CNN models: Resnet-50, and VGG-19 are used as feature extractors for CA classification in eye dataset. The following sub-sections discuss the essential structure of each adopted CNN architecture.

#### 2.3.1. Residual neural network

Residual neural network (Resnet) is a well-known pre-trained model that took first place in the ImageNet Large-scale visual recognition challenge (ILSVRC) classification competition in 2015, with a top-five error rate of 3.57% [32]. A brief architecture of ResNet-50 is shown in Figure 9. The network is separated into four stages, except stage 1, each of which has a convolutional block and an identity block. Each convolutional block and identity block had three 1x1 and 3x3 convolutional layers and one 1x1 convolutional layer. Convolution, batch normalisation, rectified linear regularisation unit (ReLU), and maximum pooling are among the four layers that make up Stage 1. Finally, there is an average pooling layer, a fully connected layer, and a SoftMax activation function in the network. As part of the fine-tuning technique, in this study, the last entirely interconnected layers were changed, and the entire network was retrained. Resnet model was fine-tuned with 50 layers on the augmented training set to classify the iris dataset. Fine-tuning starts with removing the fully connected layer of the ResNet-50 and then remodelling it to three fully connected layers with two output neurons at the output layer which correlate to the number of dataset class (normal and CA) and 50% dropout layer. The network was trained using the Adam optimization algorithm approach with a batch size of 20 images for each iteration. To reduce the problem of overfitting, the error and performance rate on validation images were observed. The ResNet-50 was found to achieve the highest training accuracy and best performance at epoch 10. The underlying architecture of fine-tune Resnet is illustrated in the Figure 10.

#### 2.3.2. Visual geometry group network

Visual Geometry Group Network namely VGGNet is similarly to AlexNet, but with additional convolutional layers. VGGNet consists of 13 convolutional layers, equalisation layers, pooling layers, and 3 fully connected layers [31]. A brief architecture of VGG-19 is shown in Figure 11. The fine-tuning of VGG-19 was done by remodelling it to three fully connected layers with two output neurons at the shallow layer of the model which corresponds to the number of labels and removing the original softmax layer and replacing it with our own. The network was trained using the Adam optimization algorithm, with each iteration using a batch size of 20 photos. The error and performance rates on the validation images were observed to avoid the problem of overfitting. The underlying model of fine-tune Resnet is shown in the Figure 12.

#### 2.3.3. Convolutional neural network (proposed method)

This section describes the model architecture and training settings for the CNN used to classify normal and CA images. Extensive testing is performed to determine the best learning parameters that improve the neural network. The CNN architecture employed for the classification of CA images is shown in Figure 13. In this study, all convolutional operations are carried out with convolutional filters of size 3x3 with zero

padding; all pooling operations are carried out with max-pooling windows of size 5×5; input images for the model are 32×32. In developing the proposed architecture, we consider the size of the available training data to build a learning model that is significantly regularized. For example, we use batch normalization and dropout training techniques, which have been shown to improve model generalization and reduce overfitting. To optimize the proposed model, we use minibatch over Adam optimization algorithm; we use a batch size of 20. Furthermore, we use a learning rate of 0.001 and train the model for 10 epochs. The learning curve for the trained CNN. The average validation accuracy is 98.81%. The proposed system for identification of CA is tested with some CA images obtained from different sources available online. The experimental results show that the developed CA identification framework is able to classify the normal and CA images with an average of 98.81% accuracy. Unlike previous works in which the suggested approach is trained and tested on the same dataset, the method proposed in this paper was trained and validated on one dataset before being tested on a completely other dataset and producing promising results.

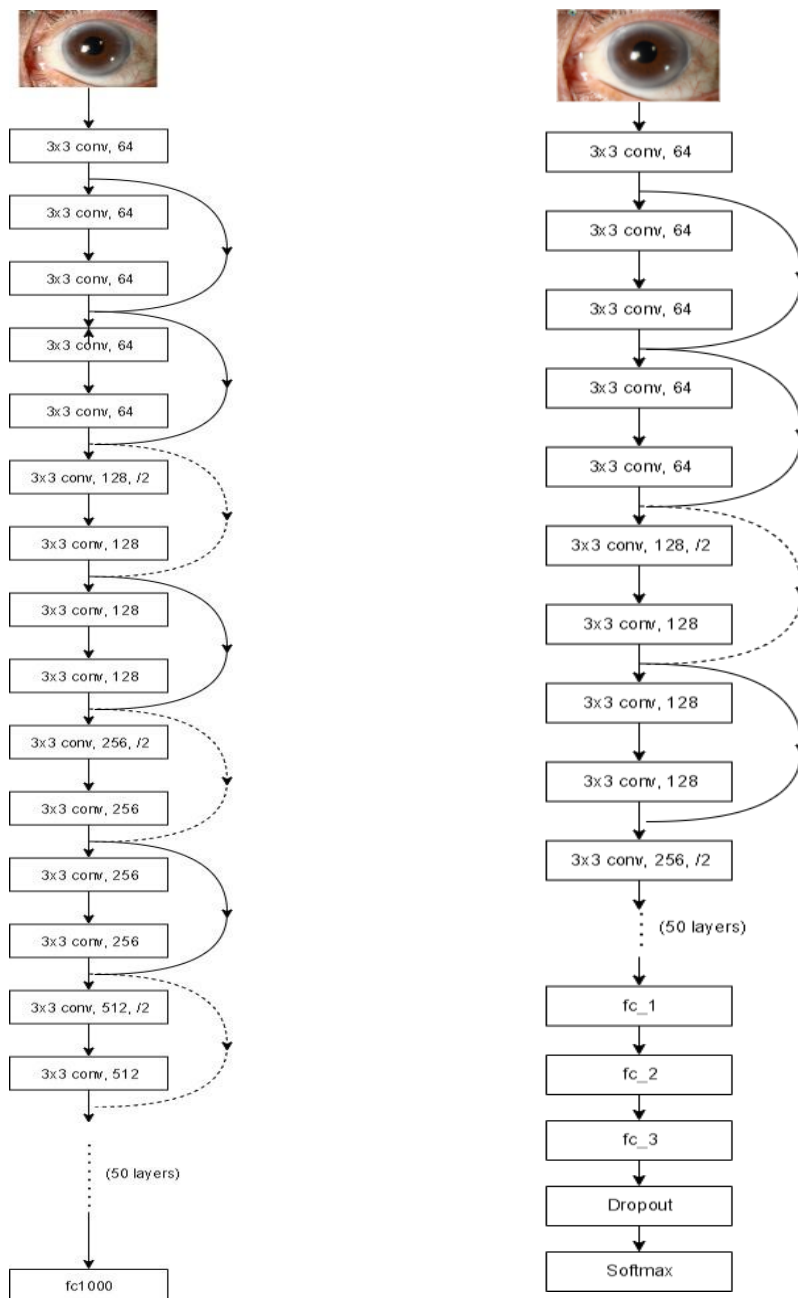


Figure 9. The brief architecture of ResNet-50    Figure 10. The fine-tuning of ResNet-50 architecture

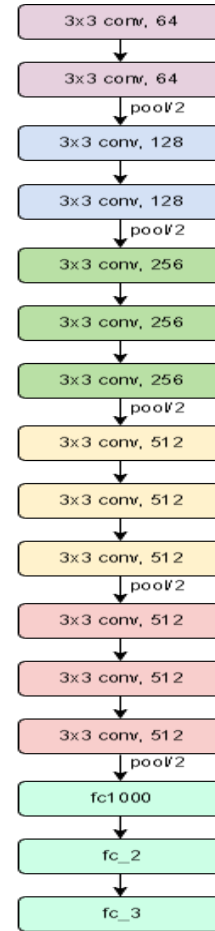
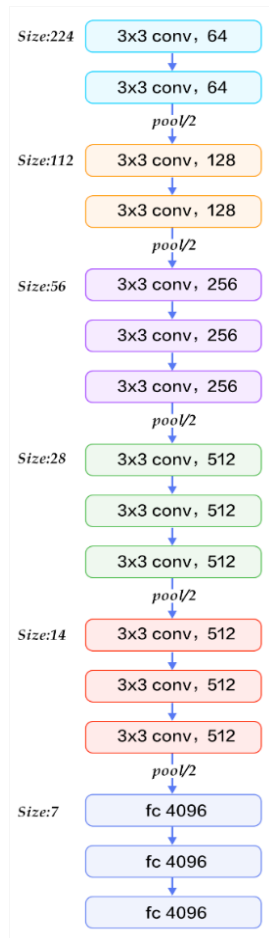


Figure 11. The brief architecture of VGG-19    Figure 12. The fine-tuning of VGG-19 architecture

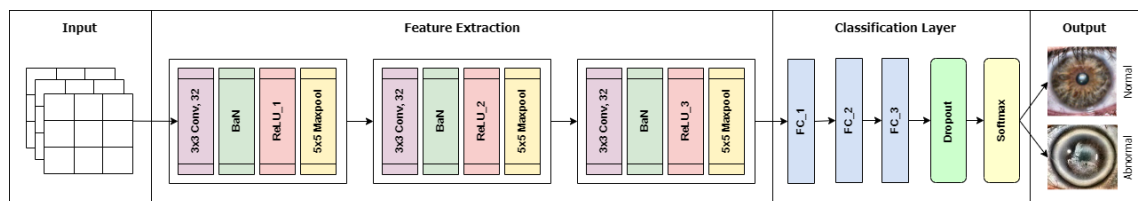


Figure 13. CNN architecture (proposed method)

### 3. RESULTS AND DISCUSSION

In this study, we investigated the suitability of a state-of-the-art deep convolutional neural network for CA identification using images. We focused on fine-tuning Resnet-50, VGG19 and CNN with 180, 49, and 19 layers respectively. Each CNN's training and block wise fine-tuning takes roughly 12-30 minutes, depending on the parameters chosen for training and fine-tuning, appropriate convergence, training validation accuracy, and error. VGG-19 model took more than 30 minutes in classifying CA whereas Resnet-50 and CNN took less than 15 minutes as shown in Table 1.

Table 1. The average execution time of training in each model

Model	Time Elapsed (s)
Resnet50	784.7
VGG19	1822.8
CNN (Proposed method)	658.8

Therefore, the classification of CA using deep learning method is challenging and time consuming. We examine the improvement of training validation accuracy and error to determine the optimal convergence of each CNN by observing the validation accuracy and error. If no improvement detected, the training is automatically terminated. In this research, all models: CNN (proposed method), Resnet-50 and VGG-19 was evaluated using performance measures in calculating the classification accuracy, as in (10) generated from the confusion matrix which is the total number of correct predictions divided by the total number of predictions as depicted in Figure 14.

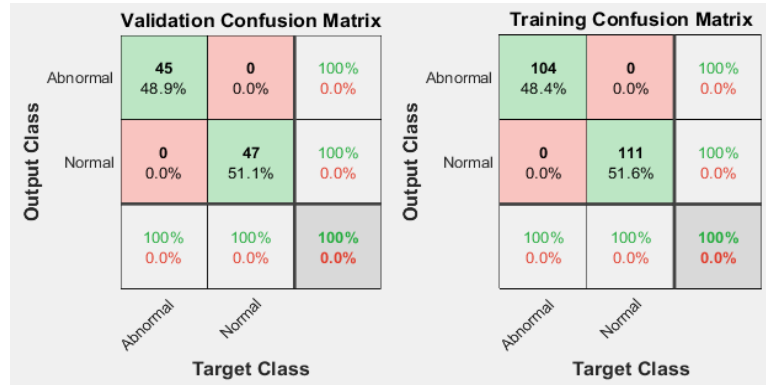


Figure 14. The sample of confusion matrix from CNN model

$$\text{Accuracy} = \frac{\text{TP} + \text{TN}}{\text{TP} + \text{FP} + \text{TN} + \text{FN}} \tag{10}$$

where TP=True Positive, TN=True Negative, FP=False Positive, FN=False Negative.

According to the training result in Table 2, Resnet50 and CNN outperform VGG-19 on a consistent basis, at a certain point, the training and validation losses both reduce and stabilise with increased number of iterations as shown in Figures 15. The CNN (proposed method) learning and loss curves as shown in Figure 15(a). The Resnet-50 learning and loss curves as shown in Figure 15(b), The VGG-19 learning and loss curves as shown in Figure 15(c). For the 1<sup>st</sup> iteration, CNN achieved better training accuracy of 82.0% with the training loss of 1.34124. When the number of iterations increase, Resnet50 achieved the highest training accuracy in classifying the CA. Overall, good accuracy results were achieved on all model with more than 80% training accuracy and significantly reduced training loss even after the 50th training iteration except for VGG19.

Table 2. The average accuracy and loss of training per iteration

Model	Iteration	Training Accuracy %	Training Loss
Resnet50	1	78.5	0.36315
	50	86.5	0.19794
	<b>100</b>	<b>88.5</b>	<b>0.19225</b>
VGG19	1	46.0	2.26557
	50	60.0	2.77418
	100	73.5	1.28786
CNN (Proposed method)	1	82.0	1.34124
	50	85.5	0.18368
	100	87.0	0.19178

The Resnet-50 and VGG-19 architectures each obtain an average classification accuracy of 98.91 percent, and 76.52 percent, respectively, as shown in Table 3, whereas the suggested method achieves an accuracy of 97.525 percent. All models had over 80% testing accuracy after fine-tuning with 10 epochs, except VGG-19. CNN (proposed method) had the best training accuracy and lowest training loss of 0.19178 followed by lowest execution time achieved compared to the other models, while VGG19 performed poorly with the least accuracy and highest training loss. Even though CNN achieved the best result, Resnet50



achieved classification accuracy of 98.04% slightly difference with the CNN model. In comparison to the three architectures, these results suggest that the CNN (proposed method) achieves excellent accuracy in CA identification and classification.

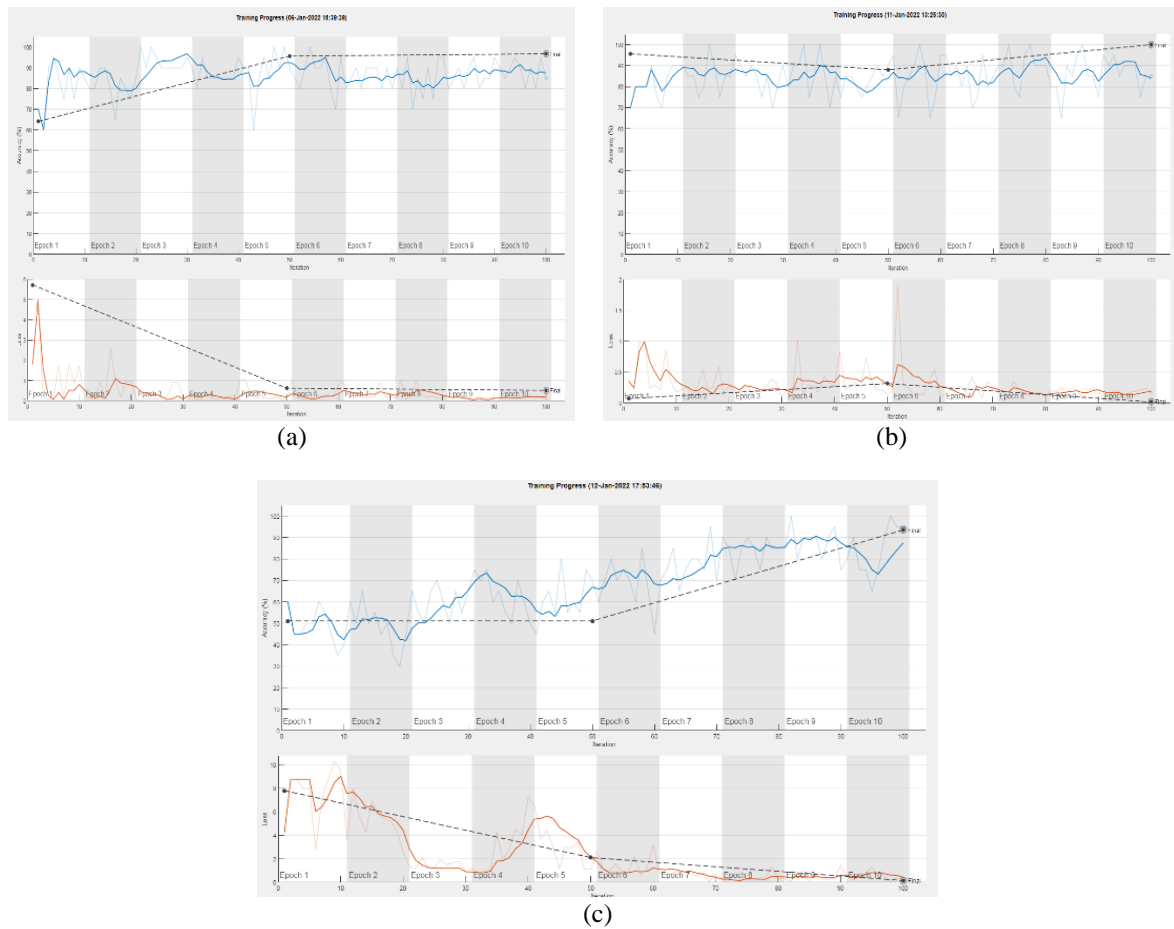


Figure 15. A sample of graph from training progress (a) the CNN (proposed method) learning and loss curves, (b) the Resnet-50 learning and loss curves, and (c) the VGG-19 learning and loss curves

Table 3. The classification accuracy (%) for each model in each fold.

	1	2	3	4	5	6	7	8	9	10	Avg. Accuracy
Resnet50	98.91	100	98.00	98.00	97.83	99.00	97.83	100	91.00	100	98.04%
VGG19	81.52	82.00	51.00	83.00	92.39	87.00	51.09	83.70	61.00	93.48	76.52%
CNN (Proposed method)	96.74	100	100	100	97.83	100	98.91	97.83	100	96.74	98.81%

#### 4. CONCLUSION

In this paper, we proposed a non-invasive technique for detecting cholesterol based on the representation of convolutional neural network (CNN) models utilizing 300 normal and 300 CA eye images from UBIRIS and medical online images respectively. The ResNet-50 network achieved satisfactory results when compared with other models. Moreover, the best result was demonstrated by the proposed pre-trained CNN model created from scratch with 10-fold cross-validation, producing high average detection in terms of accuracy at 98.0%. Compared to previous CNN research, a deep learning approach methodology considerably improved the accuracy of CA screening in this study. Even though the performance of the architecture is good, further study is needed to optimize the time execution and include larger databases to determine its effect on the classification process. This technique also can be used to diagnose eye problems caused by several types of eye diseases such as cataract, glaucoma, diabetes, tumors, and pterygium.

## ACKNOWLEDGEMENTS

We would like to thank to Universiti Teknikal Malaysia Melaka (UTeM) and Advanced Sensors & Embedded Control System Research Group (ASECs) for supporting us in accomplishing this study.




## REFERENCES

- [1] N. Amini and A. Ameri, "A deep learning approach to automatic recognition of arcus senilis," *Journal of Biomedical Physics and Engineering*, vol. 10, no. 4, pp. 507–512, Aug. 2020, doi: 10.31661/jbpe.v0i0.2003-1080.
- [2] L. Berggren, "Iridology: a critical review," *Acta Ophthalmologica*, vol. 63, no. 1, pp. 1–8, May 1985, doi: 10.1111/j.1755-3768.1985.tb05205.x.
- [3] P. J. Morrison, "The iris - A window into the genetics of common and rare eye diseases," *Ulster Medical Journal*, vol. 79, no. 1, pp. 3–5, 2010.
- [4] A. Fernández, A. Sorokin, and P. D. Thompson, "Corneal arcus as coronary artery disease risk factor," *Atherosclerosis*, vol. 193, no. 2, pp. 235–240, Aug. 2007, doi: 10.1016/j.atherosclerosis.2006.08.060.
- [5] F. L. Urbano, "Ocular Signs of Hyperlipidemia," *Hospital Physician*, no. November, pp. 51–54, 2001.
- [6] J. J. Wang, B. E. Chua, P. Mitchell, and E. Rochtchina, "Corneal Arcus and hyperlipidemia: findings from an older population," *American journal of ophthalmology*, vol. 137, no. 2, pp. 363–365, 2002.
- [7] D. Meyer, P. H. Liebenberg, and F. J. Maritz, "Serum lipid parameters and the prevalence of corneal arcus in a dyslipidaemic patient population," *Cardiovascular Journal of South Africa*, vol. 15, no. 4, pp. 166–169, 2004.
- [8] "Atlas entry-corneal arcus (Arcus Senilis).," *The University of Iowa licensed under a Creative Commons Attribution-NonCommercial-NoDerivs 3.0 Unported License. (n.d.)*. <https://eyerounds.org/atlas/pages/Arcus/index.htm> (accessed Aug. 15, 2022).
- [9] T. Kocejko, J. Ruminski, M. Mazur-Milecka, M. Romanowska-Kocejko, K. Chlebus, and K.-H. Jo, "Using convolutional neural networks for corneal arcus detection towards familial hypercholesterolemia screening," *Journal of King Saud University - Computer and Information Sciences*, Sep. 2021, doi: 10.1016/j.jksuci.2021.09.001.
- [10] V. L. Patel *et al.*, "The coming of age of artificial intelligence in medicine," *Artificial Intelligence in Medicine*, vol. 46, no. 1, pp. 5–17, May 2009, doi: 10.1016/j.artmed.2008.07.017.
- [11] T. Laksanasopin *et al.*, "A smartphone dongle for diagnosis of infectious diseases at the point of care," *Science Translational Medicine*, vol. 7, no. 273, p. 273re1, Feb. 2015, doi: 10.1126/scitranslmed.aaa0056.
- [12] C. Castaneda *et al.*, "Clinical decision support systems for improving diagnostic accuracy and achieving precision medicine," *Journal of Clinical Bioinformatics*, vol. 5, no. 1, p. 4, Dec. 2015, doi: 10.1186/s13336-015-0019-3.
- [13] M. Polsinelli, L. Cinque, and G. Placidi, "A light CNN for detecting COVID-19 from CT scans of the chest," *Pattern Recognition Letters*, vol. 140, pp. 95–100, Dec. 2020, doi: 10.1016/j.patrec.2020.10.001.
- [14] M. F. Aslan, M. F. Unlarsen, K. Sabanci, and A. Durdu, "CNN-based transfer learning–BiLSTM network: A novel approach for COVID-19 infection detection," *Applied Soft Computing*, vol. 98, p. 106912, Jan. 2021, doi: 10.1016/j.asoc.2020.106912.
- [15] A. Musha, A. Al Mamun, A. Tahabilder, J. Hossen, B. Jahan, and S. Ranjbari, "A deep learning approach for COVID-19 and pneumonia detection from chest X-ray images," *International Journal of Electrical and Computer Engineering*, vol. 12, no. 4, pp. 3655–3664, Aug. 2022, doi: 10.11591/ijece.v12i4.pp3655-3664.
- [16] Z. A. Khalaf, S. S. Hammadi, A. K. Mousa, H. M. Ali, H. R. Alnajjar, and R. H. Mohsin, "Coronavirus disease 2019 detection using deep features learning," *International Journal of Electrical and Computer Engineering*, vol. 12, no. 4, pp. 4364–4372, Aug. 2022, doi: 10.11591/ijece.v12i4.pp4364-4372.
- [17] R. A. Ramllee, S. K. Subramaniam, S. B. Yaakob, A. S. F. Rahman, and N. M. Saad, "Corneal arcus classification for hyperlipidemia detection using gray level co-occurrence matrix features," *Journal of Physics: Conference Series*, vol. 1432, no. 1, p. 012084, Jan. 2020, doi: 10.1088/1742-6596/1432/1/012084.
- [18] L. B. Rachman and Basari, "Detection of cholesterol levels by analyzing iris patterns using backpropagation neural network," *IOP Conference Series: Materials Science and Engineering*, vol. 852, no. 1, p. 012157, Jul. 2020, doi: 10.1088/1757-899X/852/1/012157.
- [19] M. Daniel, J. Raharjo, and K. Usman, "Iris-based image processing for cholesterol level detection using gray level co-occurrence matrix and support vector machine," *Engineering Journal*, vol. 24, no. 5, pp. 135–144, Sep. 2020, doi: 10.4186/ej.2020.24.5.135.
- [20] S. H. Putri and A. H. Saputro, "Design of convolutional neural network modeling for low-density lipoprotein (LDL) levels measurement based on iridology," in *ICICoS 2020 - Proceeding: 4th International Conference on Informatics and Computational Sciences*, Nov. 2020, pp. 1–5, doi: 10.1109/ICICoS51170.2020.9299102.
- [21] C. Banowati, A. Novianty, and C. Setianingsih, "Cholesterol level detection based on iris recognition using convolutional neural network method," in *2019 IEEE Conference on Sustainable Utilization and Development in Engineering and Technologies, CSUDET 2019*, Nov. 2019, pp. 116–121, doi: 10.1109/CSUDET47057.2019.9214690.
- [22] I. M. M. Yusoff, R. Yahya, W. R. W. Omar, and L. C. Ku, "Non invasive cholesterol meter using Near Infrared sensor," in *Proceedings - 2015 Innovation and Commercialization of Medical Electronic Technology Conference, ICMET 2015*, Nov. 2016, pp. 100–104, doi: 10.1109/ICMETC.2015.7449581.
- [23] M. Milanić, A. Bjorgan, M. Larsson, P. Marraccini, T. Strömberg, and L. L. Randeberg, "Hyperspectral imaging for detection of cholesterol in human skin," in *Optical Diagnostics and Sensing XV: Toward Point-of-Care Diagnostics*, Mar. 2015, vol. 9332, p. 93320W, doi: 10.1117/12.2076796.
- [24] K. G. Adi and P. V. Rao, "A non-invasive method of detection of cholesterol by level set segmentation and ANN as classifier using MLP-BP and RBF.," *International Journal on Advanced Electrical and Computer Engineering (IJAECE)*, vol. 3, no. 3, pp. 28–31, 2016.
- [25] P. Sethupriyan, "Identification and Cholesterol estimation of skin using hand pattern image," *International Journal of Advanced Research in Electrical, Electronics and Instrumentation Engineering (An ISO, vol. 3297, 2007, doi: 10.15662/IJAREEIE.2015.0408151.*
- [26] H. Proença, S. Filipe, R. Santos, J. Oliveira, and L. A. Alexandre, "The UBIRIS.v2: A database of visible wavelength iris images captured on-the-move and at-a-distance," *IEEE Transactions on Pattern Analysis and Machine Intelligence*, vol. 32, no. 8, pp. 1529–1535, Aug. 2010, doi: 10.1109/TPAMI.2009.66.




- [27] J. S. Yoo, J. H. Choi, K. S. Choi, D. Y. Lee, H. Y. Kim, and J. O. Kim, "Fast search of a similar patch for self-similarity-based image super resolution," *IEICE Transactions on Information and Systems*, vol. E99D, no. 8, pp. 2194–2198, 2016, doi: 10.1587/transinf.2016EDL8049.
- [28] J. Ma, X. Fan, S. X. Yang, X. Zhang, and X. Zhu, "Contrast limited adaptive histogram equalization-based fusion in YIQ and HSI Color Spaces for Underwater Image Enhancement," *International Journal of Pattern Recognition and Artificial Intelligence*, vol. 32, no. 7, p. 1854018, Jul. 2018, doi: 10.1142/S0218001418540186.
- [29] S. M. Pizer *et al.*, "Adaptive histogram equalization and its variations.," *Computer vision, graphics, and image processing*, vol. 39, no. 3, pp. 355–368, Sep. 1987, doi: 10.1016/S0734-189X(87)80186-X.
- [30] S. U. Khan, N. Islam, Z. Jan, I. Ud Din, and J. J. P. C. Rodrigues, "A novel deep learning-based framework for the detection and classification of breast cancer using transfer learning," *Pattern Recognition Letters*, vol. 125, pp. 1–6, Jul. 2019, doi: 10.1016/j.patrec.2019.03.022.
- [31] H. Mujtaba, "Introduction to resnet or residual network. greatlearning blog: free resources what matters to shape your career!" <https://www.mygreatlearning.com/blog/resnet/> (accessed Aug. 04, 2021).

## BIOGRAPHIES OF AUTHORS






**Nur Farahin Bt Abdul Halim**    is a Master candidate from the Faculty of Computer and Electrical Engineering, Universiti Teknikal Malaysia Melaka (UTeM). She received her BSc Honors Degree in Computer Science (Artificial Intelligence) from UTeM. Her current research interest includes artificial intelligence, image processing, statistical analysis using machine learning. She can be contacted at email: m022010012@student.utem.edu.my.






**Ir. Dr. Ridza Azri Bin Ramlee**    is a Senior Lecturer in Faculty of Computer and Electrical Engineering, UTeM. He holds a Bachelor Engineering (Electrical) Hons. in 2000 and MScs in Telecommunication and Information Engineering in 2008 from University Teknologi MARA, Malaysia. He was awarded as Doctorate in communications and network engineering from Universiti Putra Malaysia in 2019. He also obtains the corporate member MIEM and professional engineer with practicing certificate (PEPC) BEM since 2012. He has total 20 years of working experience as a Biomedical Engineer at Pusat Perubatan UKM and as a lecturer at UTeM. He can be contacted at email: ridza@utem.edu.my.



**Ts. Dr. Mohd Zaki Bin Mas'ud**    is a Senior Lecturer in Computer and Communication System, teaching theory and practical in Honours Core Subject, IT and Network Security. Zaki obtained his Bachelor of Engineering (Hons) Electronic from Multimedia University (MMU) and Masters in IT (Computer Science) from Universiti Kebangsaan Malaysia (UKM). He can be contacted at email: zaki@utem.edu.my.



**Amirul Bin Jamaludin**    is a Master candidate from the Faculty of Computer and Electrical Engineering, UTeM. He received his BSc Honors Degree in Mechatronics Engineering from UTeM. His research interests include SLAM, robotics, control and machine learning. He can be contacted at email: m022010042@student.utem.edu.my.